

Visibility stacking in the quest for SNIa radio emission.

P. Hancock^{1,2}, B. M. Gaensler^{1,2} and T. Murphy^{1,2,3}

¹*Sydney Institute for Astronomy (SIfA), School of Physics, The University of Sydney, NSW 2006, Australia*

²*ARC Centre of Excellence for All-sky Astrophysics (CAASTRO)*

³*School of Information Technologies, The University of Sydney, NSW 2006, Australia*

Paul.Hancock@sydney.edu.au

ABSTRACT

We describe the process of stacking radio interferometry visibilities to form a deep composite image and its application to the observation of transient phenomena. We apply “visibility stacking” to 46 archival Very Large Array observations of nearby type Ia supernovae (SNeIa). This new approach provides an upper limit on the SNIa ensemble peak radio luminosity of $1.2 \times 10^{25} \text{erg s}^{-1} \text{Hz}^{-1}$ at 5 GHz, which is 5–10 times lower than previously measured. This luminosity implies an upper limit on the average companion stellar wind mass loss rate of $1.3 \times 10^{-7} M_{\odot} \text{yr}^{-1}$. This mass loss rate is consistent with the double degenerate scenario for SNeIa and rules out intermediate and high mass companions in the single degenerate scenario. In the era of time domain astronomy, techniques such as visibility stacking will be important in extracting the maximum amount of information from observations of populations of short lived events.

Subject headings: stars: supernovae: general — techniques: interferometric

1. Introduction

Type Ia supernovae (SNeIa) have been important to astronomy since their identification as standard candles, and subsequent use in measuring the accelerating expansion of the universe (Riess et al. 1998; Perlmutter et al. 1999). The current uncertainties in measuring cosmological parameters are dominated by systematic rather than statistical errors (Neill et al. 2006). Hence, in order to better confine the cosmological parameters it is important to understand the origin and evolution of SNeIa (Hillebrandt & Niemeyer 2000).

Recent work has been of an empirical nature, characterizing the differences between SNIa light curves as a function of environment (Hamuy et al. 2000), redshift, and metallicity (Timmes et al. 2003). Another approach is to understand the physics of a SNIa explosion from a fundamental level so that the shape and luminosity of the light curve, and its subsequent evolution, can be predicted and understood more completely. One

of the key parameters affecting the light curve evolution is the amount of circumstellar material (CSM) that is present.

As well as causing optical extinction, the expected CSM provides a medium with which the supernova (SN) ejecta can interact and produce radio synchrotron emission. This process observed in type II and Ib/c SN. The spectral and temporal distribution of this emission has been used to explore the environment and history of the progenitor systems (Montes et al. 1998). Despite the usefulness of this approach in characterizing the progenitor system, the radio detection of SNeIa has remained elusive.

The mechanism by which SNIa white dwarf progenitors obtain a critical mass of $\sim 1.4 M_{\odot}$ is thought to be either accretion from, or merger with, a binary companion. In the single degenerate (SD) scenario, a CO white dwarf accretes material from a companion star which is losing mass via Roche-lobe overflow or strong stellar wind (Whelan & Iben 1973; Nomoto 1982). In the dou-

ble degenerate (DD) scenario, two white dwarfs coalesce and ignite (Webbink 1984; Iben & Tutukov 1984). In both cases the strength of the radio emission depends on the density of the CSM which is in turn dependent on the density of the progenitor stellar wind. The shocked CSM can also produce X-ray emission which can be used to probe the CSM. Immler et al. (2006) claimed to have detected X-ray emission from the shocked CSM of the SNIa 2005ke, however this was not confirmed by Hughes et al. (2007).

Many projects have searched for radio emission from SNeIa, but no detection has been made (Eck et al. 2002, 1995; Weiler et al. 1989). The largest set of radio observations of SNeIa is collected by Panagia et al. (2006). In the SD scenario the current lack of a radio detection has placed constraints on the companion mass loss rate, and restricted the mass of a post main-sequence companion to be relatively low. At even lower luminosity and mass loss rates, the solely-SD scenario becomes untenable, whilst a radio detection of a SNIa would dis-confirm the solely-DD scenario which predicts no such emission. Radio observations of SNeIa can thus be used to determine whether or not all SNeIa result from only the SD or DD scenario, and can probe the ratio of SD to DD progenitors, in the case of a mixed population.

More sensitive measurements can be obtained from deeper observations, or via a combination of currently available observations. Stacking is the technique of combining observations or images to form a composite, and is the two dimensional equivalent of forming a weighted average. Stacking can be used to extract the average properties of a population of sources that are too faint to be detected individually and has been used at γ -ray (Aleksić et al. 2011), X-ray (Laird et al. 2010), optical (White et al. 2007), infrared and radio (Garn & Alexander 2009) wavelengths.

This letter is organized as follows: §2 outlines the process of stacking and introduces visibility stacking, §3 describes the data selection and reduction process, §4-5 present and discuss the results of the visibility stacking, and conclusions are drawn in §6.

2. Visibility Stacking

Traditionally stacking involves forming calibrated images of a single source which are then weighted and combined to produce a more sensitive image. For N observations, each with an integration time of t , and Gaussian noise with an rms σ , a weighting scheme of $w = 1/\sigma^2$ will result in a combined image with rms noise of σ/\sqrt{N} , which is equivalent to a single observation of total length $T = N \cdot t$. Such a stacking scheme is commonly used to break long observations into multiple shorter ones, to mitigate against problems such as radio interference, cosmic rays, and time-dependent calibration schemes, depending on the wavelength of observation. Non-Gaussian or correlated noise signals will result in a stacked image with a noise that is above the ideal σ/\sqrt{N} , and different weighting schemes are required to account for such problems.

Imaging radio synthesis observations involves a conversion between the visibility and image domains. The visibility sampling function (or (u, v) coverage) of a radio interferometer is incomplete and generally non-uniform. Incomplete (u, v) coverage will cause the reconstructed image to deviate from the true radio sky, with some spatial scales being under represented or absent. This problem is well known and motivates the design and layout of radio observatories (Thompson 1999) including the Very Large Array (VLA, Thompson et al. 1980), Australia Telescope Compact Array (ATCA, Frater et al. 1992), the Low Frequency Array (LOFAR, Röttgering 2003) and the Australian Square Kilometer Array Pathfinder (ASKAP, Johnston et al. 2009). A common method for combating incomplete (u, v) coverage is to combine observations that have complimentary (u, v) coverages. For fixed arrays such as LOFAR and ASKAP this can be achieved with earth rotation synthesis, while movable arrays such as the VLA and the ATCA can also use multiple configurations. This commonly used process is the trivial case of stacking observations of a single object that are temporally separated.

Stacking of radio images of a population of sources can be done in the same manner as stacking at other wavelengths (in the image domain, Garn & Alexander 2009; Hodge et al. 2008; White et al. 2007), however incomplete (u, v) cov-

erage can cause problems. Observations that are obtained from different configurations of a telescope, will have a different (u, v) coverage and thus be sensitive to a different range of spatial scales and have different resolutions. An isolated point source can be easily detected at all spatial scales so stacking in the image domain will still recover the source. However, the noise statistics of the image is not easily understood. In more complicated fields, the distribution of sources and their morphologies become confused with spatial sampling effects and confident detections are difficult.

It is possible to benefit from improved (u, v) coverage as well as the lower noise gained from a longer integration time by using a technique we term visibility stacking. Visibility stacking is achieved by combining visibilities from observations of a population of sources *before* the image is created.

When stacking in the image domain it is important to ensure that the input images are free of confusing sources, and the target source positions are aligned. The same is true for visibility stacking, but these corrections need to be applied to the visibility data. Removing confusing sources can be achieved by subtracting appropriate models from the visibility data. Aligning the target source positions can be achieved by adjusting the phases of the visibilities.

3. Target selection

Observations of 27 nearby ($z < 0.1$) SNeIa have been carried out by Panagia et al. (2006) using the VLA at wavelengths between 0.7 and 20 cm from 1981 to 2003. This data set has a large number of SNIa observations from a single instrument and a consistent set of calibrators making it ideal for forming a stacked image.

The data set is not completely homogeneous, with the VLA configuration being restricted by the observing season. The archival observations cover all standard configurations of the VLA (A, B, C, D, AnB, BnC, CnD), and are spread across multiple frequencies. In order to obtain the most sensitive stacked image, the 6 cm observations were used as they constituted 75 of the 148 observations.

3.1. Data reduction

The raw data were obtained from the VLA archive¹, converted into uvfits format with AIPS (Greisen 2003), and reduced in MIRIAD (Sault et al. 1995). Flagging was based on manual inspection. In keeping with the analysis of Panagia et al. (2006), 3C286 was used as a primary calibrator for each of the observations. The flux of the primary calibrator varied by less than 1% over the course of the observing period.

A number of observations that were listed by Panagia et al. (2006) were not used in the final stacked image due to problems with: data access (4 could not be located in the VLA archive), data quality (6 had poor or missing calibrator observations, 4 had incorrect gains), or complicated field sources (15 observations, 8 of which include Centaurus A). The total number of usable observations was thus reduced to 46, and are listed in Table 1.

In many cases the field of view of the VLA included background radio sources that created side-lobes and artefacts at the expected SNIa position which needed to be removed. A model of the sources was removed from affected visibilities. Column 4 of Table 1 lists the rms noise of individual observations when naturally weighted and with background sources removed.

Visibility stacking was achieved in MIRIAD by adjusting the phase center of each image to be at the coordinates of the target SN, and imaging with the task INVERT. Many of the observations contained two 50 MHz bands, 4.885 and 4.835 GHz (and one observation at 4.889 GHz), each of which were calibrated separately. A total of 79 such bands were used in the creation of the stacked images.

3.2. Interpretation

Images created via visibility stacking require some interpretation. In order to retain the greatest image sensitivity, the visibilities were naturally weighted when imaging. The flux in the image can thus be interpreted as being from a source at an effective distance d_0 , which is a weighted average of the input source distances. The weighting function for d_0 is then the same as for the visibility

¹<https://archive.nrao.edu/archive/advquery.jsp>

Table 1: Archival VLA observations used in the stacking analysis.

Name	Obs Date	Age	$\sigma_{6cm}\mu\text{Jy}$	dist	Name	Obs Date	Age	$\sigma_{6cm}\mu\text{Jy}$	dist
SN	Y-M-D	days	beam ⁻¹	Mpc	SN	Y-M-D	days	beam ⁻¹	Mpc
1981B	1981-Mar-11	18	82	16.6	1986O	1987-Feb-12	72	57	28
"	1981-Apr-9	46	105	"	"	1987-Apr-11	130	68	"
"	1982-Jun-25	489	31	"	"	1987-May-24	173	67	"
"	1982-Oct-2	587	50	"	"	1987-Aug-28	269	52	"
1982E	1985-Dec-29	1417	44	23.1	"	1989-Jul-17	958	90	"
1983G	1983-May-27	72	131	17.8	1987D	1987-May-15	46	108	30
1984A	1984-Mar-5	430	109	17.4	"	1987-Jun-4	66	124	"
1985A	1985-Feb-1	49	93	26.8	"	1987-Jun-21	83	32	"
"	1985-Feb-17	65	65	"	"	1987-Sep-18	172	62	"
"	1986-Jun-15	550	71	"	"	1988-May-29	426	174	"
"	1987-Oct-23	1045	104	"	1987N	1987-Dec-20	37	91	37.0
1985B	1985-Feb-22	70	173	28.0	"	1988-Feb-1	76	84	"
"	1985-Mar-18	94	50	"	"	1988-Mar-31	135	55	"
"	1985-Sep-15	275	74	"	"	1988-Aug-22	279	64	"
"	1986-Apr-30	502	81	"	1989B	1989-Feb-2	10	38	11.1
"	1987-Sep-18	1008	56	"	"	1989-Feb-3	11	27	"
1986A	1986-Feb-7	18	126	46.1	"	1989-Mar-6	42	39	"
"	1986-Feb-25	36	89	"	"	1989-Mar-27	63	57	"
"	1986-Mar-16	55	38	"	"	1989-Apr-6	73	64	"
"	1986-Apr-3	73	51	"	1989M	1990-Feb-13	271	64	17.4
"	1986-Jun-15	146	67	"	"	1990-May-29	376	65	"
"	1987-Apr-1	436	68	"	1992A	1993-Feb-5	400	53	24.0
					1994D	1994-May-4	57	35	14
					1998bu	1999-Jan-7	245	67	11.8

Table 2: Parameters for the stacked images. Radio luminosity and inferred mass loss rates are 3σ upper limits.

	Image Stack		
	Early	Late	All
d_o (Mpc)	14.3	19.0	15.7
Effective Age (Days)	51.9	478	251
Effective Integration at 50 MHz b/w (hr)	22.5	19.6	42.1
1σ ($\mu\text{Jy beam}^{-1}$)	16.7	19.2	13.3
Synthesized beam (arcsec ²)	21×18	22×15	21×17
L_o (erg s ⁻¹ Hz ⁻¹)	1.2×10^{25}	2.5×10^{25}	1.2×10^{25}
\dot{M} ($M_{\odot}\text{yr}^{-1}$)	1.3×10^{-7}	1.5×10^{-6}	5.4×10^{-7}

data:

$$\frac{1}{d_0^4} = \frac{\frac{N_1}{d_1^4} + \frac{N_2}{d_2^4} + \dots + \frac{N_m}{d_m^4}}{N_1 + N_2 + \dots + N_m} \quad (1)$$

where N_i is the number of visibilities in i^{th} observation, and d_i is the distance to the corresponding source. The function is of the form N_i/d_i^4 since doubling the integration time doubles N_i and increases the sensitivity by $\sqrt{2}$ which allows a source of the same luminosity to be seen at a distance $\sqrt[4]{2}$ times further away.

Using Equation (1), it is possible to calculate the effective distance probed by a stacked image, and convert the flux density of a detection or upper limit into an ensemble luminosity or luminosity limit. Distances listed in Table 1 are from Panagia et al. (2006), and were used to calculate the effective distance d_0 for the stacked image.

A similar weighting function was applied to the age of a SN at the time of its observation to obtain an effective age that corresponds to the luminosity calculated in the above-mentioned manner. The relevant weighting function is:

$$\text{Age} = \frac{\text{Age}_1 \cdot N_1 + \text{Age}_2 \cdot N_2 + \dots + \text{Age}_m \cdot N_m}{N_1 + N_2 + \dots + N_m} \quad (2)$$

4. Results

The 46 usable observations were combined to make three stacked images of the SNe. Two images were formed by selecting only observations with an age of either less than 100 days (Early) or greater than 100 days (Late), respectively. A

third image was created using all of the available observations (All). In all three images no emission was seen above 3σ at the location of the SNe. The representative distance, age and corresponding luminosity of each of these images are listed in Table 2, and are plotted in Figure 1 along with the upper limits obtained from the individual observations.

The stacked image of all observations represents a 50 MHz band width equivalent integration time of 42.1 hours, longer than any previous radio observation of any individual SNIa.

The final stacked images were not completely without structure and some faint sources were detected away from the expected SN location. Stacked images were created for each of the host galaxies, and faint sources that were not able to be seen or removed from the short observations were detectable in the more sensitive stacked image. These sources were found to be HII regions within, and the core of, NGC 3627 and were previously noted by Eck et al. (2002).

Following Panagia et al. (2006, 2011), we model the luminosity of the SNIa as:

$$\frac{L_{\nu}}{10^{26}\text{erg s}^{-1}\text{Hz}^{-1}} = \Lambda \left(\frac{\dot{M}/10^{-6}M_{\odot}\text{yr}^{-1}}{w_{\text{wind}}/10\text{km s}^{-1}} \right)^{1.65} \times \left(\frac{\nu}{5\text{GHz}} \right)^{-1.1} \left(\frac{t}{1\text{day}} \right)^{-1.5} e^{-\tau_{CSM}}, \quad (3)$$

where t is the time since explosion, or age of the SN. The parameter Λ is a dimensionless constant. On the assumption that the light curves of SNeIa

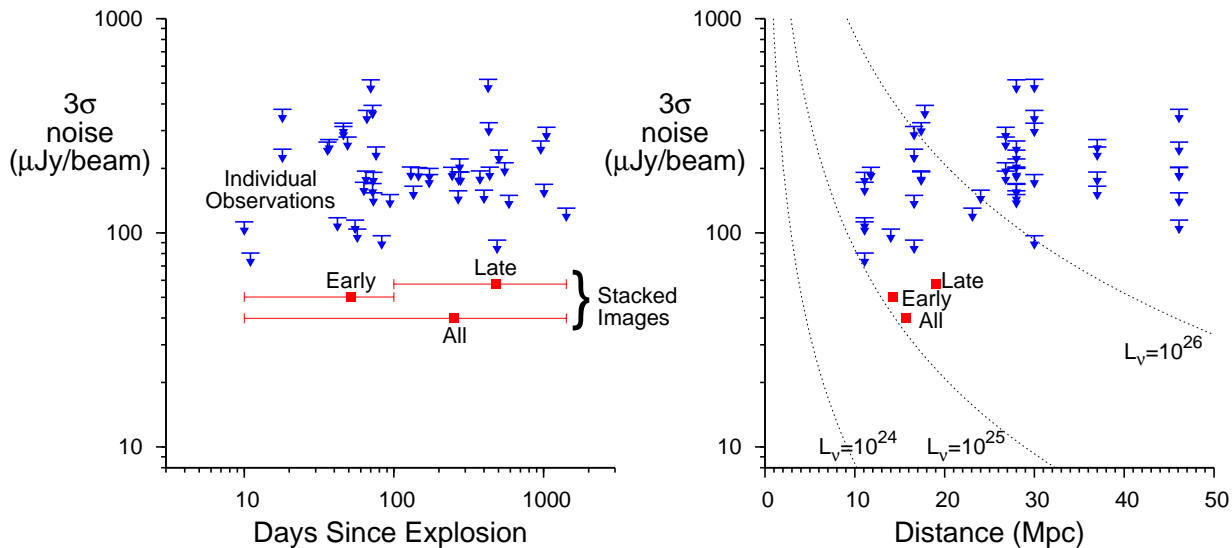


Fig. 1.— The 3σ noise of the individual and stacked images as a function of SN age and distance. Three stacked images were created – Early, All and Late. In each stacked image the noise level is fainter than in the individual observations. *Left*: The noise in each image as a function of the age of the SNe at the time of observation. *Right*: The noise in each image as a function of SN distance. Lines have been drawn to show the 3σ upper limit for different 5 GHz luminosities in $\text{erg s}^{-1}\text{Hz}^{-1}$.

are similar to that of SNeIb/c, we take $\Lambda = 1285 \pm 245$ as calculated by Panagia et al. (2006). The value of Λ can vary by a factor of 10 depending on which set of SNe are used in the derivation, however the dependence of L_ν on \dot{M}/w_{wind} results in an uncertainty in \dot{M} of less than a factor of 2. A wind velocity $w_{\text{wind}} = 10 \text{ km s}^{-1}$ was assumed, consistent with a post main-sequence companion in the SD scenario. This model assumes that the CSM has a radial density profile $\rho \propto r^{-2}$.

The optical depth τ_{CSM} of the CSM external to the blast wave depends on absorption mechanism (free-free or synchrotron self absorption), as well as the structure of the CSM (clumpy or uniform). Constant among all considerations of optical depth is that the luminosity peaks when the optical depth is unity. With the assumption $\tau_{\text{CSM}} = 1$, equation (3) was used to estimate an upper limit for the mass loss rate \dot{M} , as listed in Table 2.

5. Discussion

Combining data from different observations is a common technique for making measurements for a population of sources, however when dealing with upper limits care needs to be taken. A combined

upper limit on the radio luminosity of SNeIa studied here can be obtained by creating a weighted average of the individual upper limits without stacking. Whilst this will result in a combined upper limit that is consistent with that obtained from a stacked image, it does not allow for the detection of sources. Stacking images permits the detection of source which would otherwise be below the detection limit, whilst combining upper limits implicitly assumes that no such detection will be made.

The stacked 5 GHz images provide upper limits to the ensemble radio flux of SNeIa which are fainter than the individual observations. The stacked images of Early and All observations both have a 3σ upper limit on the 5 GHz luminosity of $1.2 \times 10^{25} \text{ erg s}^{-1} \text{ Hz}^{-1}$ which is the same as that of the best observation of SN1989B (1989-Feb-03). Whilst the stacked images are more sensitive than the individual observations (see Fig 1 left), the fact that $L_\nu \propto \sigma d^2$ means that the flux/distance combination of the single observation and stacked image both correspond to the same luminosity limit ($1.2 \times 10^{25} \text{ erg s}^{-1} \text{ Hz}^{-1}$ Fig 1 right). Rearranging Equation 3 with $L_\nu \propto \sigma d^2$, we find that $\dot{M} \propto \sigma^{0.61} d^{1.2} t^{0.93}$, so that the limit on mass loss rate is more strongly dependent on the distance of

the SN and age of observation than its sensitivity. Since the observation of SN1989B was made when it was only 10 days old, and the source is at only 11.1 Mpc, it provides a lower limit on the companion mass loss rate ($3.1 \times 10^{-8} M_{\odot} \text{yr}^{-1}$) than the older and more distant Early stacked image ($1.3 \times 10^{-7} M_{\odot} \text{yr}^{-1}$) even though the Early stacked image is more sensitive.

However, while the SN1989B observation provides an upper limit on SN luminosity which is the same as Early and All stacked images, it is only applicable to SN1989B and is not representative of the underlying population. If SNeIa are a completely homogeneous population of sources then this limit may be applied to all SNeIa, however the optical luminosity differences seen by Hamuy et al. (2000) and Timmes et al. (2003) suggest that this is not the case. By creating a stacked image of the SNeIa we are able to claim a luminosity limit which is applicable to all SNe within the sample, and be more confident that it is applicable to SNeIa as a whole. The 3σ luminosity limits and mass loss rates reported by Panagia et al. (2006)² have a median of $1.2 \times 10^{26} \text{erg s}^{-1} \text{Hz}^{-1}$ and $6.2 \times 10^{-7} M_{\odot} \text{yr}^{-1}$ respectively. The ensemble luminosity limits for the Early, Late and All stacked images are 5 – 10 times lower these earlier limits, and the ensemble mass loss rate constraints of the Early and All stacked images are up to 5 times lower.

If the solely-SD scenario is correct then the mass transfer from the companion to the WD must result in some residual mass that is not accreted, our observations limit this contribution to the CSM to a rate of less than $1.3 \times 10^{-7} M_{\odot} \text{yr}^{-1}$. Wind accretion onto a binary companion is typically $\sim 10\%$ efficient (Yungelson et al. 1995), implying a companion mass loss rate of $\leq 1.4 \times 10^{-7} M_{\odot} \text{yr}^{-1}$ ruling out red giants and medium to high mass ($2-10 M_{\odot}$) post main-sequence stars as the possible binary companion. A main-sequence companion, having winds $\gg 10 \text{km s}^{-1}$, could remain undetected even with much higher mass loss rates. Accretion via Roche-lobe overflow (RLOF) is more efficient than wind accretion and the models of Hachisu et al. (1999) predict that SNeIa formed from RLOF of a $1.3-2 M_{\odot}$ red giant on to a

CO white dwarf are consistent with the measured mass loss rate. The solely-SD scenario (with a red giant or post main-sequence companion $\geq 2 M_{\odot}$) is thus not able to account for the properties of the observed SNIa population. A detailed analysis of the formation of binary systems with large mass ratios ($5-8 M_{\odot}$ primary, $< 2 M_{\odot}$ secondary) is beyond the scope of this paper, but such systems may be relatively rare because of the amount of mass transfer from the primary to the companion during the final stages of its evolution.

6. Conclusions

By employing the new technique of visibility stacking we were able to create more sensitive images of SNeIa. The corresponding 3σ limits on the ensemble radio luminosity are considerably lower than most of the limits of Panagia et al. (2006). Since the calculated mass loss rate depends on the distance and age of the SN as well as the sensitivity of the observation, we were unable to obtain an ensemble limit on \dot{M} that was lower than the individual observation of SN1989B on Feb 3rd 1989. However, we were able to place an overall stringent limit on the ensemble 5 GHz radio luminosity and mass loss rate for the SNIa population of $1.2 \times 10^{25} \text{erg s}^{-1} \text{Hz}^{-1}$ and $1.3 \times 10^{-7} M_{\odot} \text{yr}^{-1}$ respectively. By creating visibility stacked images of SNeIa we conclude that the solely single degenerate scenario (with a red giant or post main-sequence companion $\geq 2 M_{\odot}$) cannot account for the observed SNIa population.

Visibility stacking is a powerful tool for analyzing radio observations of transient sources. The use of visibility stacking can be extended to the radio properties of any sample of radio quiet or radio faint sources, where image domain stacking has previously been used. The increased sensitivity can increase the confidence with which detections and upper limits are made. This technique needs to be applied carefully in the analysis of transient sources when such phenomena may result from more than one progenitor scenario.

In the era of time domain astronomy there will be a focus on obtaining more sensitive measurements on populations of sources that are transient. Such sources do not afford the luxury of repeated observations and thus techniques such as visibility stacking will be important in investigating source

²Their 2σ upper limits have been converted to 3σ limits for comparison.

populations.

In studies which hope to detect the radio emission of SNeIa by increasing the sensitivity of the observations (eg, Chomiuk et al. 2011), the ability to form visibility stacked images will further increase the sensitivity and applicability of the observations.

Acknowledgments

The National Radio Astronomy Observatory is a facility of the National Science Foundation operated under cooperative agreement by Associated Universities, Inc. This research has been supported by the Australian Research Council through grants DP0987072 and FS100100033, and through the Science Leveraging Fund of the New South Wales Office for Science and Medical Research. The Centre for All-sky Astrophysics is an Australian Research Council Centre of Excellence, funded by grant CE11E0090.

Facilities: VLA

REFERENCES

- Aleksić, J., et al. 2011, ApJ, 729, 115
- Chomiuk, L., Soderberg, A. M., Chevalier, R., Badenes, C., & Fransson, C. 2011, BAAS, 43
- Eck, C. R., Cowan, J. J., & Branch, D. 2002, ApJ, 573, 306
- Eck, C. R., Cowan, J. J., Roberts, D. A., Boffi, F. R., & Branch, D. 1995, ApJ, 451
- Frater, R. H., Brooks, J. W., & Whiteoak, J. B. 1992, JEEEA, 12, 103
- Garn, T., & Alexander, P. 2009, MNRAS, 394, 105
- Greisen, E. W. 2003, AIPS, the VLA, and the VLBA, ed. A. Heck, Vol. 285 (Dordrecht, The Netherlands: Kluwer Academic Publishers), 109–126
- Hachisu, I., Kato, M., & ichi Nomoto, K. 1999, ApJ, 522, 487
- Hamuy, M., Trager, S. C., Pinto, P. A., Phillips, M. M., Schommer, R. A., Ivanov, V., & Suntzeff, N. B. 2000, AJ, 120, 1479
- Hillebrandt, W., & Niemeyer, J. C. 2000, ARA&A, 38, 191
- Hodge, J. A., Becker, R. H., White, R. L., & de Vries, W. H. 2008, AJ, 136, 1097
- Hughes, J. P., Chugai, N., Chevalier, R., Lundqvist, P., & Schlegel, E. 2007, ApJ, 670, 1260
- Iben, I. J., & Tutukov, A. V. 1984, ApJS, 54, 335
- Immler, S., et al. 2006, ApJ, 648, L119
- Johnston, S., Feain, I. J., & Gupta, N. 2009, The Low-Frequency Radio Universe ASP Conference Series, 407
- Laird, E. S., Nandra, K., Pope, A., & Scott, D. 2010, MNRAS, 401, 2763
- Montes, M. J., Van Dyk, S. D., Weiler, K. W., Sramek, R. A., & Panagia, N. 1998, ApJ, 506, 874
- Neill, J. D., et al. 2006, AJ, 132, 1126
- Nomoto, K. 1982, ApJ, 253, 798
- Panagia, N., Dyk, S., Weiler, K., Sramek, R., Stockdale, C., & Murata, K. 2006, ApJ, 646, 369
- . 2011, ApJ, 733, 72
- Perlmutter, S., et al. 1999, ApJ, 517, 565
- Riess, A. G., et al. 1998, AJ, 116, 1009
- Röttgering, H. J. A. 2003, NewAR, 47, 405
- Sault, R. J., Teuben, P. J., & Wright, M. C. H. 1995, in Astronomical Society of the Pacific Conference Series, Vol. 77, Astronomical Data Analysis Software and Systems IV, ed. R. Shaw, H. Payne, & J. Hayes, 433
- Thompson, A. R. 1999, in Astronomical Society of the Pacific Conference Series, Vol. 180, Synthesis Imaging in Radio Astronomy II, ed. G. B. Taylor, C. L. Carilli, & R. A. Perley, 11
- Thompson, A. R., Clark, B. G., Wade, C. M., & Napier, P. J. 1980, ApJS, 44, 151
- Timmes, F. X., Brown, E. F., & Truran, J. W. 2003, ApJ, 590, L83

Webbink, R. F. 1984, *ApJ*, 277, 355

Weiler, K. W., Panagia, N., Sramek, R. A., van der Hulst, J. M., Roberts, M. S., & Nguyen, L. 1989, *ApJ*, 336, 421

Whelan, J., & Iben, I. J. 1973, *ApJ*, 186, 1007

White, R. L., Helfand, D. J., Becker, R. H., Glikman, E., & de Vries, W. 2007, *ApJ*, 654, 99

Yungelson, L., Livio, M., Tutukov, A., & Kenyon, S. J. 1995, *ApJ*, 447, 656